Proposal for enhanced photon blockade in parity-time-symmetric coupled microcavities

Jiahua Li (李家华),[1,2,*] Rong Yu (余荣),[3,†] and Ying Wu (吴颖)[4,‡]

[1]*Wuhan National Laboratory for Optoelectronics and School of Physics, Huazhong University of Science and Technology, Wuhan 430074, People's Republic of China*

[2]*Key Laboratory of Fundamental Physical Quantities Measurement of Ministry of Education, Wuhan 430074, People's Republic of China*

[3]*Hubei Province Key Laboratory of Intelligent Robot, School of Science, Wuhan Institute of Technology, Wuhan 430073, People's Republic of China*

[4]*School of Physics, Huazhong University of Science and Technology, Wuhan 430074, People's Republic of China*

(Received 6 September 2015; published 16 November 2015)

Recent demonstrations of parity-time- ($\mathcal{PT}$-) symmetric structure have exhibited the great potential of this system for tailoring the light-matter interaction and developing a wide range of robust quantum devices. Here we explore the second-order photon correlations in a $\mathcal{PT}$-symmetric system consisting of a passive nonlinear cavity coupled to an active cavity via optical tunneling. It is shown numerically that strong photon antibunching including perfect photon blockade can be obtained efficiently even if the Kerr nonlinearity strength, the photon-tunneling strength, and the driving strength are smaller than the cavity decay rate. The physical mechanism underlying photon blockade originally comes from the dynamical enhancement of intracavity nonlinearity by the effect of supermode field localization in the $\mathcal{PT}$-symmetric arrangement. The results obtained provide insight into the crossover between the photon blockade and $\mathcal{PT}$-symmetric theory. Such controllable photon antibunching may find applications in the generation of high-quality single-photon sources.

DOI: 10.1103/PhysRevA.92.053837 PACS number(s): 42.50.Ct, 42.50.Ar, 11.30.Er, 42.50.Dv

I. INTRODUCTION

Photon blockade and tunneling is a current research topic and is important for a variety of fundamental studies and practical applications [1–13]. Experimentally, the signature of the photon blockade and tunneling can be distinguished by measuring the second-order correlation function at time delay zero $g^{(2)}(0)$ [14]. For the photon blockade (or photon antibunching $g^{(2)}(0) < 1$), the presence of a single photon in a system, driven by an external coherent field, will hinder the coupling of the subsequent photons because of the strong nonlinearities present in the quantum system itself. In contrast, for the photon tunneling (or photon bunching $g^{(2)}(0) > 1$), the coupling of initial photons will favor the coupling of the subsequent photons [14]. The observation of photon blockade relies on a challenging task that nonlinear interactions in quantum systems exceed the characteristic dissipation rate. A key point for high-quality single-photon sources is to realize a strong photon blockade [15–17]. Thus, in order to achieve the best photon blockade, considerable research effort has been spent in a variety of strongly coupled quantum systems including cavity, optomechanics, and circuit quantum electrodynamics [18–26].

Since the conception of parity-time ($\mathcal{PT}$) symmetry was proposed originally in quantum mechanics [27,28], photonics has been proved to be an excellent platform for exploring new ideas and developing practical techniques arising from all kinds of $\mathcal{PT}$-symmetric structures. An interesting property of $\mathcal{PT}$-symmetric systems is that they may have purely real eigenvalue spectra in some domains of the parameter spaces (this situation is referred to as an unbroken $\mathcal{PT}$-symmetric phase) despite their Hamiltonian non-Hermiticity [28]. In addition, these systems undergo an abrupt $\mathcal{PT}$ phase transition where the systems lose the corresponding $\mathcal{PT}$ symmetry. At a so-called exceptional point (EP), pairs of eigenvalues collide and become complex. Typically, the transition from an unbroken $\mathcal{PT}$-symmetric phase (real eigenvalue spectra below the EP) to a spontaneous $\mathcal{PT}$-symmetry breaking (complex eigenvalue spectra above the EP) can appear when the system parameter in the Hamiltonian is properly tuned [29–31]. The $\mathcal{PT}$-symmetric physics that follows from such non-Hermitian properties has enabled applications such as low-power optical isolation [32–35], the single-mode microcavity laser [36–38], loss-induced or gain-induced transparency [39,40], power oscillations violating left-right symmetry [41], unidirectional invisibility [42–44], efficient phonon lasing or diodes [45,46], ultralow-threshold optical chaos [47], and high-sensitivity metrology [48]. However, the crossover between the photon blockade and $\mathcal{PT}$-symmetric theory remains largely unexplored. The following are the questions that we will address. Can the $\mathcal{PT}$-symmetric theory influence the photon blockade significantly? How is the photon blockade modified in such a $\mathcal{PT}$-symmetric system? The results obtained may stimulate further investigations and applications in the regimes of low-power nonlinear and quantum optics [49].

The organization of the paper is as follows. In Sec. II we establish the theoretical model and present the Hamiltonian of the optical $\mathcal{PT}$ system consisting of two coupled cavities, one of which has loss (passive cavity) and weak nonlinearity and the other gain (active cavity) but no nonlinearity. In Sec. III we study in detail the second-order photon correlations by tuning the system parameters and provide the corresponding physical explanation in the supermode picture. In Sec. IV we comment on the feasibility of implementing our theoretical method in this $\mathcal{PT}$-symmetric system. In Sec. V we summarize our results.

*huajia_li@163.com
†rong_yu2013@163.com
‡yingwu2@126.com

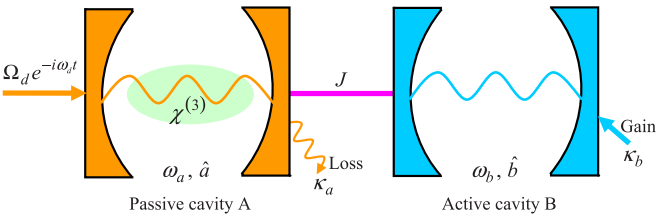

FIG. 1. (Color online) Schematic illustration of $\mathcal{PT}$-symmetric coupled cavities including a passive nonlinear cavity A (resonance frequency ω_a and cavity mode $\hat{a}$) coupled to an active cavity B (resonance frequency ω_b and cavity mode $\hat{b}$) with tunneling strength J. The passive cavity A includes Kerr nonlinear materials [1,5,8,50] and is coherently driven by an external monochromatic laser field with strength Ω_d and frequency ω_d. Here κ_a and κ_b are, respectively, the cavity decay rate and gain rate.

II. PROPOSED $\mathcal{PT}$-SYMMETRIC SYSTEM AND REVIEW OF $\mathcal{PT}$-SYMMETRIC THEORY

Spurred by recent studies in optical $\mathcal{PT}$ devices [33,34,36–38], we consider a passive nonlinear cavity coupled to an active cavity via optical tunneling, i.e., the $\mathcal{PT}$-symmetric double cavity (see Fig. 1), for realizing the strong photon-blockade effect. In the presence of a driving laser, the Hamiltonian for the system reads (setting $\hbar = 1$)

$$\mathcal{H} = (\omega_a - i\kappa_a/2)\hat{a}^\dagger\hat{a} + (\omega_b - i\kappa_b/2)\hat{b}^\dagger\hat{b} + J(\hat{a}\hat{b}^\dagger + \hat{a}^\dagger\hat{b}) + U_{nl}\hat{a}^\dagger\hat{a}^\dagger\hat{a}\hat{a} + (\Omega_d\hat{a}^\dagger e^{-i\omega_d t} + \Omega_d^*\hat{a}e^{i\omega_d t}), \quad (1)$$

where $\hat{a}$ ($\hat{b}$) is the bosonic operator eliminating a photon in the passive (active) cavity A (B) with resonance frequency ω_a (ω_b); $U_{\rm nl}$ is the Kerr nonlinear interaction strength from the passive cavity A, which arises from optical nonlinearity of the underlying material, such as an optical cavity embedding a Kerr optical medium [1,5,8,50]; J is the photon-tunneling strength between the two cavities and can be tuned by changing the distance between them; and Ω_d is the real strength of the external driving field with carrier frequency ω_d. In addition, $\kappa_a = \kappa_a^i + \kappa_a^e$ is the total loss rate of the passive cavity A, which contains an intrinsic loss rate κ_a^i and an external coupling loss rate κ_a^e. In an active cavity B, on the other hand, the effective loss rate $\kappa_b = \kappa_b^i - \xi$ is reduced by the gain ξ (round-trip energy gain). Whether $\kappa_b > 0$ (loss) or $\kappa_b < 0$ (gain) depends on ξ. Specifically, $\kappa_a > 0$ and $\kappa_b > 0$ correspond to a passive-passive double cavity, whereas $\kappa_a > 0$ and $\kappa_b < 0$ define a passive-active (i.e., $\mathcal{PT}$-symmetric) double cavity, which have been realized in recent experiments [33,34,36–38].

Before proceeding further, it is instructive to briefly illustrate the principal mechanism behind $\mathcal{PT}$ symmetry in our studied system. Under the condition of a very weak nonlinearity $U_{\rm nl}$ and switching off the driving field $\Omega_d = 0$, we take into account the first three terms in Eq. (1) to look into the $\mathcal{PT}$ phase transition point, with the result

$$\mathcal{H} = (\hat{a}^\dagger\ \hat{b}^\dagger)\begin{pmatrix}\omega_a - i\kappa_a/2 & J\\ J & \omega_b - i\kappa_b/2\end{pmatrix}\begin{pmatrix}\hat{a}\\ \hat{b}\end{pmatrix}. \quad (2)$$

Here it should be pointed out that the nonlinear Kerr term $U_{\rm nl}\hat{a}^\dagger\hat{a}^\dagger\hat{a}\hat{a}$ in Eq. (1) may lead to an EP shift between the $\mathcal{PT}$-symmetric phase and the broken-$\mathcal{PT}$ phase. However, the nonlinearity-induced shift of the EP can be ignored because the Kerr nonlinearity $U_{\rm nl}$ in our proposed model is very weak. In the following, for convenience, we define P as the above 2×2 matrix $P \equiv \left(\begin{smallmatrix}\omega_a - i\kappa_a/2 & J\\ J & \omega_b - i\kappa_b/2\end{smallmatrix}\right)$, D as the 2×2 diagonal matrix $D \equiv \left(\begin{smallmatrix}\omega_- & 0\\ 0 & \omega_+\end{smallmatrix}\right)$, and Q as the 2×2 transformation matrix $Q \equiv \left(\begin{smallmatrix}Q_{11} & Q_{12}\\ Q_{21} & Q_{22}\end{smallmatrix}\right) = (|q_-\rangle \quad |q_+\rangle)$ with $|q_-\rangle = \left(\begin{smallmatrix}Q_{11}\\ Q_{21}\end{smallmatrix}\right)$ and $|q_+\rangle = \left(\begin{smallmatrix}Q_{12}\\ Q_{22}\end{smallmatrix}\right)$. Then the above Hamiltonian can be diagonalized as

$$\mathcal{H} = (\hat{a}^\dagger\ \hat{b}^\dagger)Q\underbrace{Q^{-1}PQ}_{D}Q^{-1}\begin{pmatrix}\hat{a}\\ \hat{b}\end{pmatrix} = (\hat{A}^\dagger\ \hat{B}^\dagger)\begin{pmatrix}\omega_- & 0\\ 0 & \omega_+\end{pmatrix}\begin{pmatrix}\hat{A}\\ \hat{B}\end{pmatrix}, \quad (3)$$

with the definition

$$\begin{pmatrix}\hat{A}\\ \hat{B}\end{pmatrix} = Q^{-1}\begin{pmatrix}\hat{a}\\ \hat{b}\end{pmatrix} \Rightarrow \begin{pmatrix}\hat{a}\\ \hat{b}\end{pmatrix} = Q\begin{pmatrix}\hat{A}\\ \hat{B}\end{pmatrix}, \quad (4)$$

where Q^{-1} is the inverse matrix of Q and $QQ^{-1} = 1$. From the relationship $Q^{-1}PQ = D$, we have the key expressions $PQ = QD \Rightarrow P|q_-\rangle = \omega_-|q_-\rangle$ and $P|q_+\rangle = \omega_+|q_+\rangle$. This implies that the so-called diagonalization or decoupling problems turn into solving the eigenvectors $(|q_-\rangle, |q_+\rangle)$ and eigenvalues (ω_-, ω_+) of the given matrix P, i.e., solving the secular equation $\det(P - \omega I) = 0$, where I is a 2×2 identity matrix. To summarize, the coupling of these two cavities creates two supermodes $\hat{A}$ and $\hat{B}$ with the corresponding eigenfrequencies ω_+ and ω_-, yielding

$$\omega_\pm = \frac{1}{2}\left(\omega_a + \omega_b - i\frac{\kappa_a + \kappa_b}{2}\right) \pm \frac{1}{2}\sqrt{4J^2 - \left[i(\omega_a - \omega_b) + \frac{\kappa_a - \kappa_b}{2}\right]^2}. \quad (5)$$

Generally, the analytical expressions of Q are too cumbersome and are not presented here.

It is clear from Eq. (5) that the two eigenfrequencies are dependent on ω_a, ω_b, κ_a, κ_b, and J. To obtain purely real eigenvalue spectra, i.e., $\mathrm{Im}(\omega_\pm) = 0$, requires the imaginary parts of $\omega_\pm$ to disappear. According to Eq. (5), when $\omega_b = \omega_a$, $\kappa_b = -\kappa_a$, and $J \geqslant \kappa_a/2$, this requirement can be well satisfied. Note that the condition $\omega_a = \omega_b = \omega_0$ shows the same cavity resonance frequencies and $\kappa_b = -\kappa_a$ corresponds to the balanced gain and loss for both cavity modes. In this case, the $\mathcal{PT}$-symmetric supermodes with a zero linewidth are spectrally distributed at $\tilde{\omega}_\pm = \pm\sqrt{J^2 - \kappa_a^2/4}$ away from the central frequency ω_0. For the case of $J = \kappa_a/2$, the two supermodes coalesce into the central frequency ω_0. For the case of $J > \kappa_a/2$, the system is in the unbroken $\mathcal{PT}$-symmetric phase. However, when $J < \kappa_a/2$, the eigenfrequencies become complex and the $\mathcal{PT}$ symmetry is spontaneously broken. As a result, $J = \kappa_a/2$ is the EP and is often referred to as the spontaneous $\mathcal{PT}$-symmetric breaking point [33,34]. As the $\mathcal{PT}$-symmetric phase is broken, one of the two supermodes gradually vanishes because of the absorption while the other experiences amplification. More generally, the EP still exists and can be defined by $J = (\kappa_a - \kappa_b)/4$ when $\omega_b = \omega_a$ for the unbalanced gain and loss $\kappa_b \neq -\kappa_a$ [31]. The threshold of symmetry breaking depends solely on the relation

between the gain or loss and photon tunneling. This $\mathcal{PT}$ phase transition can significantly influence the dynamics of the passive-active double-cavity system. It has been demonstrated experimentally that introducing optical gain to one of the two cavities balances the passive loss of the other and the transition point shows the characteristic features of an EP. For example, both Peng *et al.* [33] and Chang *et al.* [34] realized remarkable $\mathcal{PT}$-symmetric behaviors in two directly coupled whispering-gallery-mode (WGM) microtoroidal resonators by properly adjusting the gain in one active resonator and the loss in the other passive resonator. Moreover, the field localization in the passive resonator and an accompanying enhancement of optical nonlinearity leading to nonreciprocal light transmission are found in such an optical compound structure. In addition, Peng *et al.* [36], Feng *et al.* [37], and Hodaei *et al.* [38] reported an unconventional single-mode lasing by delicately manipulating the gain-to-loss ratio in the $\mathcal{PT}$-symmetric double cavity.

Transforming the above Hamiltonian (1) into the rotating frame at the frequency ω_d of the driving laser field by means of $\mathcal{H}_0 = \omega_d(\hat{a}^\dagger\hat{a} + \hat{b}^\dagger\hat{b})$, $U(t) = e^{-i\mathcal{H}_0 t} = e^{-i\omega_d t(\hat{a}^\dagger\hat{a}+\hat{b}^\dagger\hat{b})}$, and $\mathcal{H}_{\rm rot} = U^\dagger(t)\mathcal{H}U(t) - iU^\dagger(t)\frac{\partial U(t)}{\partial t} = U^\dagger(t)(\mathcal{H} - \mathcal{H}_0)U(t)$ [51], we can rewritten the system Hamiltonian (1) as

$$\mathcal{H}_{\rm rot} = (\Delta_a - i\kappa_a/2)\hat{a}^\dagger\hat{a} + (\Delta_b - i\kappa_b/2)\hat{b}^\dagger\hat{b} + J(\hat{a}\hat{b}^\dagger + \hat{a}^\dagger\hat{b}) + U_{nl}\hat{a}^\dagger\hat{a}^\dagger\hat{a}\hat{a} + \Omega_d(\hat{a}^\dagger + \hat{a}), \quad (6)$$

where $\Delta_a = \omega_a - \omega_d$ ($\Delta_b = \omega_b - \omega_d$) is the frequency detuning between the cavity mode A (B) and the related driving field. Note that the same cavity resonance frequencies $\omega_a = \omega_b = \omega_0$ lead to the same detunings $\Delta_a = \Delta_b = \Delta$. Without loss of generality, we have taken the driving strength Ω_d above to be real.

III. NUMERICAL SIMULATIONS

A. Outline of our numerical method

The dynamics of the $\mathcal{PT}$-symmetric double-cavity system can be determined by the nonlinear Schrödinger equation $i\partial|\psi(t)\rangle/\partial t = \mathcal{H}_{\rm rot}|\psi(t)\rangle$, where $|\psi(t)\rangle$ describes the quantum state of the system at time t. Here the cavity losses or gains have been included phenomenologically in the above non-Hermitian Hamiltonian [see Eq. (6)]. On the basis of Fock states (photon number states) $|n_a,n_b\rangle \equiv |n_a\rangle \otimes |n_b\rangle$, the system state $|\psi(t)\rangle$ can be expressed as $|\psi(t)\rangle = \sum_{n_a,n_b=0}^{+\infty} C_{n_a,n_b}(t)|n_a,n_b\rangle$, where $C_{n_a,n_b}(t)$ is the probability amplitude and satisfies a coupled set of differential equations by means of the above-mentioned Schrödinger equation (not shown here), n_a represents the photon number of the passive cavity mode, and n_b represents the photon number of the active cavity mode. The steady-state probability amplitude $C^{\rm ss}_{n_a,n_b}$ can be obtained by setting $\partial C_{n_a,n_b}(t)/\partial t = 0$ and then the normalized equal-time second-order correlation functions for the passive cavity field in the steady-state case can be calculated as

$$g_a^{(2)}(0) = \frac{\langle\hat{a}^\dagger\hat{a}^\dagger\hat{a}\hat{a}\rangle}{\langle\hat{a}^\dagger\hat{a}\rangle^2} = \frac{\sum_{n_a,n_b} n_a(n_a-1)\left|C^{\rm ss}_{n_a,n_b}\right|^2}{\left(\sum_{n_a,n_b} n_a\left|C^{\rm ss}_{n_a,n_b}\right|^2\right)^2}, \quad (7)$$

An alternative method involves numerically solving the exact master equation $\partial\rho/\partial t = -i[\tilde{\mathcal{H}}_{\rm rot},\rho] + \mathcal{L}\rho$, where $\tilde{\mathcal{H}}_{\rm rot} = \Delta_a\hat{a}^\dagger\hat{a} + \Delta_b\hat{b}^\dagger\hat{b} + J(\hat{a}\hat{b}^\dagger + \hat{a}^\dagger\hat{b}) + U_{\rm nl}\hat{a}^\dagger\hat{a}^\dagger\hat{a}\hat{a} + \Omega_d(\hat{a}^\dagger + \hat{a})$ excludes the cavity loss and gain, ρ is the system density matrix, and $\mathcal{L}$ is the dissipative Liouvillian superoperator given in Refs. [52–55], i.e., $\mathcal{L}\rho = \frac{\kappa_a}{2}(2\hat{a}\rho\hat{a}^\dagger - \hat{a}^\dagger\hat{a}\rho - \rho\hat{a}^\dagger\hat{a}) + \frac{\kappa_b}{2}(2\hat{b}\rho\hat{b}^\dagger - \hat{b}^\dagger\hat{b}\rho - \rho\hat{b}^\dagger\hat{b})$. The formal solution of ρ above can be given in terms of the basis $|n_a,n_b\rangle$ as $\rho(t) = \sum_{n_a,n_b}\sum_{n'_a,n'_b}\rho_{n_a,n_b;n'_a,n'_b}(t)|n_a,n_b\rangle\langle n'_a,n'_b|$ and $\rho_{n_a,n_b;n'_a,n'_b}(t) = \langle n_a,n_b|\rho(t)|n'_a,n'_b\rangle$. The steady-state density operator $\rho^{\rm ss}_{n_a,n_b;n'_a,n'_b}$ can be obtained by setting $\partial\rho(t)/\partial t = 0$. Similarly, the zero-delay-time correlation function of the steady state is defined by

$$g_a^{(2)}(0) = \frac{\langle\hat{a}^\dagger\hat{a}^\dagger\hat{a}\hat{a}\rangle}{\langle\hat{a}^\dagger\hat{a}\rangle^2} = \frac{{\rm Tr}(\rho^{\rm ss}\hat{a}^\dagger\hat{a}^\dagger\hat{a}\hat{a})}{[{\rm Tr}(\rho^{\rm ss}\hat{a}^\dagger\hat{a})]^2} = \frac{\sum_{n_a,n_b} n_a(n_a-1)\rho^{\rm ss}_{n_a,n_b;n_a,n_b}}{\left(\sum_{n_a,n_b} n_a\rho^{\rm ss}_{n_a,n_b;n_a,n_b}\right)^2}. \quad (8)$$

Obviously, $\rho^{\rm ss}_{n_a,n_b;n_a,n_b} = |C^{ss}_{n_a,n_b}|^2$, which always holds in quantum optics [56].

Two approaches can offer us the same solutions and here we demonstrate only the results obtained from the Schrödinger equation, as this method is much faster and computationally less demanding. In order to carry out fully quantum correlation function calculations via MATLAB software, we have to truncate the Hilbert space at some finite photon number that is sufficiently large that the contribution of higher-order photon number states is negligibly small (to this end, the convergence is ensured under the condition of the weak driving field). The measurement of the photon correlation function defined above can be performed by the Hanbury-Brown-Twiss technique [18,19].

B. Results for the second-order correlation function

Figure 2 presents the second-order correlation function $g_a^{(2)}(0)$ as a function of the detuning Δ/κ_a for three possible configurations: (i) a passive single nonlinear cavity (i.e., the

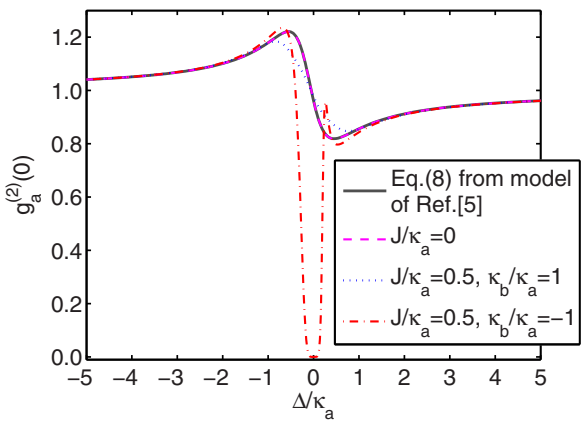

FIG. 2. (Color online) Second-order correlation function $g_a^{(2)}(0)$ as a function of the detuning Δ/κ_a between the driving field and cavity resonance. The other parameters for the simulations are chosen as $U_{\rm nl}/\kappa_a = 0.1$ and $\Omega_d/\kappa_a = 0.01$.

model considered from Ref. [5] or setting $J/\kappa_a = 0$ in the present work), (ii) a passive-passive double cavity ($J/\kappa_a = 0.5$ and $\kappa_b/\kappa_a = 1$), and (iii) a passive-active (i.e., $\mathcal{PT}$-symmetric) double cavity ($J/\kappa_a = 0.5$ and $\kappa_b/\kappa_a = -1$), respectively. For a passive single nonlinear cavity, according to Eq. (8) in the weak driving limit from Ref. [5], the second-order correlation $g_a^{(2)}(0)$ is calculated (see the black solid line in Fig. 2). The antibunching ($g_a^{(2)}(0) < 1$) is observed at positive detunings and the maximum antibunching $g_a^{(2)}(0) \sim 0.8$ is obtained for $\Delta/\kappa_a = 0.5$. At negative detunings, the bunching ($g_a^{(2)}(0) > 1$) occurs due to the driving field hitting the two-photon resonance of cavity A [5]. The maximum bunching $g_a^{(2)}(0) \sim 1.2$ is achieved for $\Delta/\kappa_a = -0.5$. When the photon-tunneling strength between the two cavities is switched off, i.e., $J/\kappa_a = 0$, the proposed model returns to the passive single nonlinear cavity in Ref. [5]. The full behavior of $g_a^{(2)}(0)$ via numerical simulation is very well reproduced by the analytic solution from Ref. [5] under the weak driving field (see the purple dashed line in Fig. 2). For a passive-passive double cavity ($J/\kappa_a = 0.5$ and $\kappa_b/\kappa_a = 1$), the bunching and antibunching effects are obviously weakened (see the blue dotted line in Fig. 2). For a $\mathcal{PT}$-symmetric double cavity ($J/\kappa_a = 0.5$ and $\kappa_b/\kappa_a = -1$), the most striking feature is the occurrence of the perfect photon blockade [$g_a^{(2)}(0) \sim 0$] because the two-photon transition is largely suppressed in comparison with the single-photon transition when the driving field is on resonance with the cavity (see the red dash-dotted line in Fig. 2).

Physically, around the spontaneous $\mathcal{PT}$-symmetric breaking point, the field localization induces the dynamical accumulations of optical energy in the two supermode-based cavities, corresponding to an increasing intracavity nonlinearity [33,34,46]. More specifically, the initial weak Kerr nonlinearity from the passive cavity is redistributed between the passive and active cavities and moreover it is enhanced by field localization of the supermodes in the $\mathcal{PT}$-broken phase. This change of optical nonlinearity gives rise to an important result that the strong photon blockade can be triggered even when the photon-tunneling strength J and the driving strength Ω_d are smaller than the cavity decay rate κ_a due to the field-localization-enhanced nonlinearity. On the other hand, it is worth emphasizing that the supermodes become almost lossless at EP in the $\mathcal{PT}$ case. The field localization is also coupled with a reduction of the optical loss of the supermodes due to the $\mathcal{PT}$ symmetry near the EP in the $\mathcal{PT}$-broken phase. In the $\mathcal{PT}$-unbroken phase, however, there is no field localization since both supermodes are intensity symmetric.

In order to explicitly show the enhancement of cavity nonlinearity in the $\mathcal{PT}$-broken regime, we focus on the nonlinear Kerr term in the Hamiltonian (6), i.e., $\mathcal{H}_{\rm nl} = U_{\rm nl}\hat{a}^\dagger\hat{a}^\dagger\hat{a}\hat{a}$, and transform $\mathcal{H}_{\rm nl}$ to a different supermode basis (namely, a so-called supermode picture). By making good use of $\hat{a} = Q_{11}\hat{A} + Q_{12}\hat{B}$ [see Eq. (4)] and dropping the nonresonant terms in the rotating frame, we can rewrite $\mathcal{H}_{\rm nl}$ in terms of these supermodes $\hat{A}$ and $\hat{B}$ as $\mathcal{H}_{\rm nl} \simeq U_1\hat{A}^\dagger\hat{A}^\dagger\hat{A}\hat{A} + U_2\hat{B}^\dagger\hat{B}^\dagger\hat{B}\hat{B} + U_3\hat{A}^\dagger\hat{A}\hat{B}^\dagger\hat{B}$, where the nonlinear coefficients are defined by $U_1 = U_{\rm nl}|Q_{11}|^4$, $U_2 = U_{\rm nl}|Q_{12}|^4$, and $U_3 = 4U_{\rm nl}|Q_{11}|^2|Q_{12}|^2$. For our considered $\mathcal{PT}$-broken case in which $\omega_a = \omega_b$ and $\kappa_a = -\kappa_b$, after performing the cumbersome algebraic calculations we find that these nonlinear coefficients satisfy $U_j \propto U_{\rm nl}J^4/(J^2 - \kappa_a^2/4 + \epsilon^2)^2$, where $j = 1,2,3$ and ε is a small quantity arising from the Kerr nonlinearity-induced shift of this boundary. Note that before reviewing the $\mathcal{PT}$-symmetric theory we omit this nonlinearity-induced shift of the $\mathcal{PT}$ phase point. Clearly, when $J \sim \kappa_a/2$ (in the vicinity of the $\mathcal{PT}$ phase transition point), these effective nonlinear coefficients are greatly enhanced. That is to say, the existing weak nonlinearity $U_{\rm nl}$ can be significantly increased by operating the system of two coupled cavities in the vicinity of the spontaneous $\mathcal{PT}$-symmetric breaking point. Compared with the previous schemes for realizing the photon blockade [1–5,7–11], our $\mathcal{PT}$-symmetric system relaxes the requirements and allows a more practical parameter range for solid-state materials.

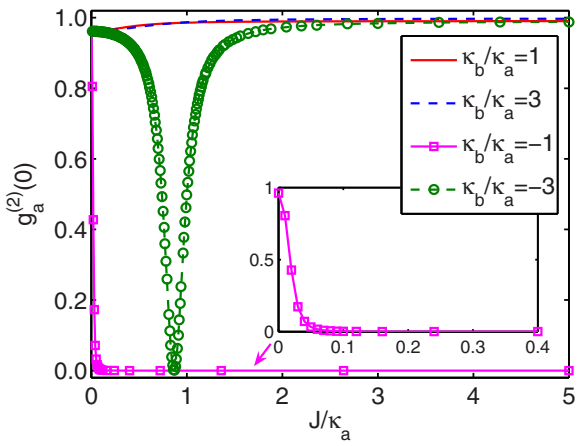

FIG. 3. (Color online) Dependence of $g_a^{(2)}(0)$ on the photon-tunneling strength J/κ_a at the detuning $\Delta/\kappa_a = 0$. The inset shows a zoom-in of $g_a^{(2)}(0)$ in a smaller region of the abscissa axis for $\kappa_b/\kappa_a = -1$. The other parameters are the same as in Fig. 2.

For further insight, it is useful to consider the effect of the photon-tunneling strength. In Fig. 3 we display how the second-order correlation function $g_a^{(2)}(0)$ explicitly depends on the photon-tunneling strength J/κ_a for four different values of the gain-to-loss ratio κ_a/κ_b. Here $\kappa_a/\kappa_b > 0$ and $\kappa_a/\kappa_b < 0$ represent, respectively, a passive-passive double cavity and a $\mathcal{PT}$-symmetric double cavity. As can be seen, $g_a^{(2)}(0) \to 1$ for $\kappa_a/\kappa_b > 0$ and $J/\kappa_a > 1$. Only a vanishingly small antibunching is obtained in the range $0 < J/\kappa_a < 1$. Moreover, increasing the loss in the second cavity B from $\kappa_b/\kappa_a = 1$ to $\kappa_b/\kappa_a = 3$ cannot change the full behavior of $g_a^{(2)}(0)$. When the gain (i.e., $\kappa_b/\kappa_a = -1$ and -3) instead of the loss (i.e., $\kappa_b/\kappa_a = 1$ and 3) is introduced into cavity B, the behaviors of $g_a^{(2)}(0)$ become significantly different. The strong photon antibunching [even the photon blockade $g_a^{(2)}(0) \to 0$] can be obtained efficiently when $J/\kappa_a < 1$. In particular, for the balanced gain and loss $\kappa_b = -\kappa_a$, $g_a^{(2)}(0) \to 0$ quite rapidly even at an arbitrary small amount of the photon-tunneling strength. Physically, this is because, in the vicinity of the gain-loss balance, a strong nonlinear relation emerges between the intracavity photon intensity and the input power [33,34].

Clearly, the efficiency of such a quantum system that is used to create the photon antibunching is strongly dependent on the effective value of the Kerr nonlinear interaction strength $U_{\rm nl}$. In Fig. 4 we show the dependence of the

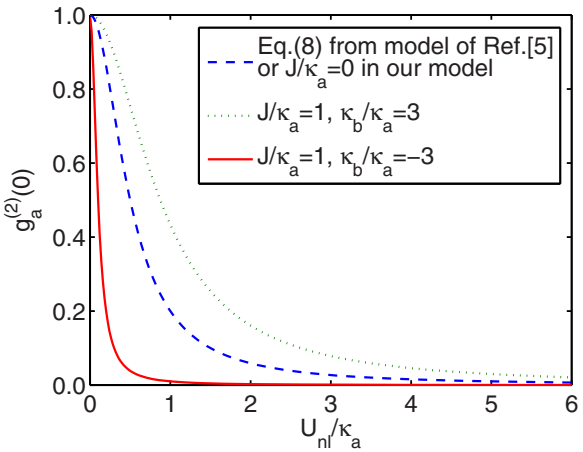

FIG. 4. (Color online) Dependence of $g_a^{(2)}(0)$ on the Kerr nonlinear interaction strength $U_{\rm nl}$ at the detuning $\Delta/\kappa_a = 0$. The other parameters are the same as in Fig. 2.

second-order correlation function $g_a^{(2)}(0)$ on $U_{\rm nl}/\kappa_a$ for the three different configurations: (i) a passive single nonlinear cavity (the model from Ref. [5] or $J/\kappa_a = 0$ in our model), (ii) a passive-passive double cavity ($J/\kappa_a = 1$ and $\kappa_b/\kappa_a = 3$), and (iii) a $\mathcal{PT}$-symmetric double cavity ($J/\kappa_a = 1$ and $\kappa_b/\kappa_a = -3$). As can be seen from this figure, $g_a^{(2)}(0) \to 0$ quickly with increasing $U_{\rm nl}/\kappa_a$ for the $\mathcal{PT}$-symmetric double cavity with respect to both the passive single nonlinear cavity and the passive-passive double cavity. As a consequence, strong photon antibunching in the $\mathcal{PT}$-symmetric double cavity can be easily obtained under a small value of $U_{\rm nl}/\kappa_a$, relaxing the requirements of Ref. [5].

IV. PHYSICAL IMPLEMENTATION OF OUR PROPOSAL

In this section we briefly discuss the experimental platform that can be used to implement our proposal. In the solid state, various coupled-cavity systems have been realized, such as microdisks, nanowires, microtoroids, microrings, and photonic crystals [57,58]. Here we consider two directly coupled WGM microtoroidal resonators (see, e.g., Refs. [33,34]). Optical WGM microtoroidal resonators trap and confine light in small volumes by total internal reflection around the perimeter of an air-dielectric interface. Thereby these features enhance the light intensity and nonlinear interaction. As in Ref. [33], one of the WGM microtoroidal resonators is fabricated from fused silica without dopants and has passive loss (a no-gain medium), where the elemental nonlinear interaction is third order in the electric field. The other microtoroid is an active resonator made from silica doped with Er^{3+} ions. By optically pumping the Er^{3+} ions with a pump laser in the 1460-nm wavelength band, one can provide optical gain to the active microtoroid in the 1550-nm wavelength band. This provides the gain to compensate for the loss and to amplify the weak signal laser in the 1550-nm band. Evanescent coupling between the two microtoroidal resonators exists only in the 1550-nm band. The resonators do not have overlapping resonance lines in the 1460-nm band, so the light from the pump laser is coupled only to the active microtoroid. That is to say, there is no coupling between the resonators in the 1460-nm band.

As a paradigmatic example, the actual values of the system parameters in relevant experiments [33] are chosen for the passive microtoroid as the wavelength $\lambda_a = 1550$ nm, the intrinsic quality factor $Q_a^i = 3 \times 10^7$, and the coupling loss $\kappa_a^e/2\pi = 4.25$ MHz corresponding to the coupling quality factor $Q_a^e \sim 4.5 \times 10^7$, which leads to $\kappa_a^i/2\pi = c/\lambda_a Q_a^i \sim 6.45$ MHz (c is the light speed in free space) and the total loss rate $\kappa_a/2\pi \sim 10.7$ MHz (here $\kappa_a = \kappa_a^i + \kappa_a^e$). Experimentally, the above parameter κ_a^e can be continuously adjusted by tuning the taper-resonator gap [57,58]. For the active microtoroid, the system parameter values are chosen as the wavelength $\lambda_b = 1550$ nm and the intrinsic quality factor $Q_b^i = 3.3 \times 10^6$, which results in $\kappa_b^i/2\pi = c/\lambda_b Q_b^i \sim 58.6$ MHz. A 1460-nm narrow-linewidth tunable laser is applied to produce an effective gain $\xi/2\pi \sim 69.3$ MHz (corresponding to the experimentally achievable condition [34]). In the active microtoroid, the effective gain is $\kappa_b/2\pi \sim -10.7$ MHz. The coupling strength between the two microtoroids is $J/2\pi \sim 5.35$ MHz, which is readily achievable in state-of-the-art resonators [33,34,36–38]. The Kerr nonlinear interaction strength from the passive microtoroid is $U_{\rm nl}/2\pi \sim 1.07$ MHz, which holds for silica glass materials. The strength of the external pump laser driving the passive microtoroid is $\Omega_d/2\pi \sim 0.107$ MHz. Also, such values have been experimentally demonstrated for other types of microcavities (such as microsphere resonators, microdisks, and microrings [57,58]) due to the fast pace of advancement of cavity design and nanostructuring capabilities.

Alternatively, a small fluctuation of the system parameter is inevitable in the process of experimental realization. In order to estimate theoretically the influence of this fluctuation clearly, in Fig. 5 we present the profiles of the second-order correlation with a fluctuation of κ_b (for example, $\pm 0.1\kappa_a$). It is obvious that the obtained results for the second-order correlation function $g_a^{(2)}(0) \sim 0$ are almost insensitive to small deviations from the exact used values mentioned above. As a consequence, it is likely to produce the required conditions within the same device [33] for realizing the enhanced photon blockade effects.

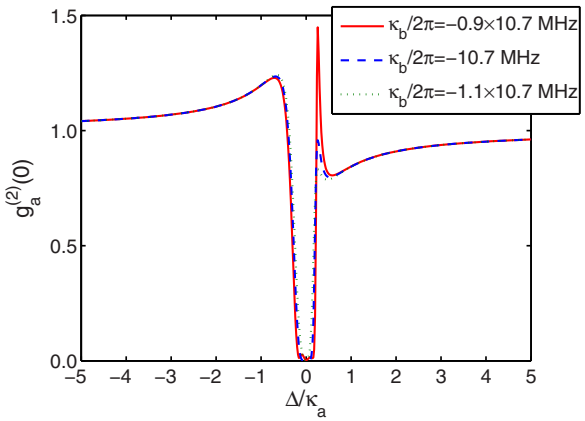

FIG. 5. (Color online) Second-order correlation function $g_a^{(2)}(0)$ as a function of the detuning Δ/κ_a between the driving field and cavity resonance for a small deviation of κ_b (for example, $\pm 0.1\kappa_a$). The other parameters for the simulations are chosen as $J/2\pi = 5.35$ MHz, $\kappa_a/2\pi = 10.7$ MHz, $U_{\rm nl}/2\pi = 1.07$ MHz, and $\Omega_d/2\pi = 0.107$ MHz, respectively.

The detection of emitted radiation and subsequent measurement of correlation functions would be performed by the Hanbury-Brown-Twiss interferometer [18,19], details depending on the geometry of the system under consideration. Finally, it should be pointed out that the present scheme may be extended to the photonic crystal cavities and other WGM resonators. Similarly, optical gain can be supplied by a solid-state quantum emitter, e.g., quantum dots or other rare-earth ions, and also through optical nonlinear Raman or parametric amplification processes.

V. CONCLUSION

We have calculated numerically the normalized second-order correlation function and discussed the photon correlation behaviors for a $\mathcal{PT}$-symmetric system of two tunnel-coupled cavities, one of which has passive loss (passive cavity A with weak nonlinearity but no optical gain) and the other optical gain (active cavity B but no nonlinearity) balancing the loss of cavity A. In contrast to a single passive nonlinear cavity or coupled passive cavities, the present $\mathcal{PT}$-symmetric double cavity features a very strong effective nonlinearity in the supermode picture, when this coupled system transits from the $\mathcal{PT}$-unbroken phase to the $\mathcal{PT}$-broken phase by properly adjusting the photon-tunneling strength or the gain-to-loss ratio [33,34,46]. Namely, the existing weak nonlinearity can be significantly increased by operating the system of two coupled cavities in the vicinity of the EP. The physical mechanism underlying this enhancement of the nonlinearity is rooted in the field localization of the supermodes generated by the two coupled cavities. In addition, this enhanced intracavity nonlinearity is almost lossless because of the gain-loss balance induced by the $\mathcal{PT}$-symmetric structure. In view of this, the proposed $\mathcal{PT}$-symmetric device can exhibit strong photon antibunching (even the perfect photon blockade) by tuning the system parameters even if the Kerr nonlinearity strength, the photon-tunneling strength, and the driving strength are smaller than the cavity decay rate. Using experimentally accessible parameter values, it was also shown that the results obtained for the second-order correlation function $g_a^{(2)}(0) \sim 0$ are insensitive to small deviations from the exact used values. The scheme proposed here may provide a promising alternative to ongoing efforts in developing integrated single-photon sources using a $\mathcal{PT}$-symmetric architecture.

ACKNOWLEDGMENTS

We appreciate the anonymous referees for their constructive comments to improve the paper. We also acknowledge Xiao-Xue Yang and Xin-You Lü for useful discussion and advice in the manuscript preparation. This research was supported in part by the National Natural Science Foundation of China (Grants No. 11375067, No. 11574104, and No. 11505131) and the National Basic Research Program of China (Contract No. 2012CB922103). R.Y. is also supported by the Youth Fund Project of Wuhan Institute of Technology (Grant No. Q201408).

[1] A. Imamoğlu, H. Schmidt, G. Woods, and M. Deutsch, Strongly Interacting Photons in a Nonlinear Cavity, Phys. Rev. Lett. **79**, 1467 (1997); K. M. Gheri, W. Alge, and P. Grangier, Quantum analysis of the photonic blockade mechanism, Phys. Rev. A **60**, R2673 (1999); A. D. Greentree, J. A. Vaccaro, S. R. de Echaniz, A. V. Durrant, and J. P. Marangos, Prospects for photon blockade in four-level systems in the N configuration with more than one atom, J. Opt. B **2**, 252 (2000); S. Rebić, A. S. Parkins, and S. M. Tan, Photon statistics of a single-atom intracavity system involving electromagnetically induced transparency, Phys. Rev. A **65**, 063804 (2002).

[2] T. C. H. Liew and V. Savona, Single Photons from Coupled Quantum Modes, Phys. Rev. Lett. **104**, 183601 (2010); O. Kyriienko and T. C. H. Liew, Triggered single-photon emitters based on stimulated parametric scattering in weakly nonlinear systems, Phys. Rev. A **90**, 063805 (2014).

[3] S. Ferretti, L. C. Andreani, H. E. Türeci, and D. Gerace, Photon correlations in a two-site nonlinear cavity system under coherent drive and dissipation, Phys. Rev. A **82**, 013841 (2010); S. Ferretti, V. Savona, and D. Gerace, Optimal antibunching in passive photonic devices based on coupled nonlinear resonators, New J. Phys. **15**, 025012 (2013).

[4] M. Bamba, A. Imamoğlu, I. Carusotto, and C. Ciuti, Origin of strong photon antibunching in weakly nonlinear photonic molecules, Phys. Rev. A **83**, 021802(R) (2011); M. Bambaa and C. Ciuti, Counter-polarized single-photon generation from the auxiliary cavity of a weakly nonlinear photonic molecule, Appl. Phys. Lett. **99**, 171111 (2011).

[5] S. Ferretti and D. Gerace, Single-photon nonlinear optics with Kerr-type nanostructured materials, Phys. Rev. B **85**, 033303 (2012).

[6] M. Bajcsy, A. Majumdar, A. Rundquist, and J. Vučković, Photon blockade with a four-level quantum emitter coupled to a photonic-crystal nanocavity, New J. Phys. **15**, 025014 (2013).

[7] I. Carusotto and C. Ciuti, Quantum fluids of light, Rev. Mod. Phys. **85**, 299 (2013).

[8] A. Majumdar and D. Gerace, Single-photon blockade in doubly resonant nanocavities with second-order nonlinearity, Phys. Rev. B **87**, 235319 (2013); A. Majumdar, C. M. Dodson, T. K. Fryett, A. Zhan, S. Buckley, and D. Gerace, Hybrid 2D material nanophotonics: A scalable platform for low-power nonlinear and quantum optics, ACS Photon. **2**, 1160 (2015).

[9] H. Flayac and V. Savona, Input-output theory of the unconventional photon blockade, Phys. Rev. A **88**, 033836 (2013).

[10] X. W. Xu and Y. Li, Tunable photon statistics in weakly nonlinear photonic molecules, Phys. Rev. A **90**, 043822 (2014).

[11] D. Gerace and V. Savona, Unconventional photon blockade in doubly resonant microcavities with second-order nonlinearity, Phys. Rev. A **89**, 031803(R) (2014).

[12] Y. H. Zhou, H. Z. Shen, and X. X. Yi, Unconventional photon blockade with second-order nonlinearity, Phys. Rev. A **92**, 023838 (2015).

[13] M.-A. Lemonde, N. Didier, and A. A. Clerk, Antibunching and unconventional photon blockade with Gaussian squeezed states, Phys. Rev. A **90**, 063824 (2014).

[14] R. Loudon, *The Quantum Theory of Light* (Oxford Science, Oxford, 2000).

[15] A. Faraon, I. Fushman, D. Englund, N. Stoltz, P. Petroff, and J. Vučković, Coherent generation of non-classical light on a chip via photon-induced tunneling and blockade, Nat. Phys. **4**, 859 (2008); A. Faraon, A. Majumdar, and J. Vučković, Generation of nonclassical states of light via photon blockade in optical nanocavities, Phys. Rev. A **81**, 033838 (2010); K. Müller, A. Rundquist, K. A. Fischer, T. Sarmiento, K. G. Lagoudakis, Y. A. Kelaita, C. S. Muñoz, E. del Valle, F. P. Laussy, and J. Vučković, Coherent Generation Of Nonclassical Light On Chip Via Detuned Photon Blockade, Phys. Rev. Lett. **114**, 233601 (2015).

[16] B. Lounis and M. Orrit, Single-photon sources, Rep. Prog. Phys. **68**, 1129 (2005).

[17] H. Flayac, D. Gerace, and V. Savona, An all-silicon single-photon source by unconventional photon blockade, Sci. Rep. **5**, 11223 (2015).

[18] K. M. Birnbaum, A. Boca, R. Miller, A. D. Boozer, T. E. Northup, and H. J. Kimble, Photon blockade in an optical cavity with one trapped atom, Nature (London) **436**, 87 (2005).

[19] A. Rundquist, M. Bajcsy, A. Majumdar, T. Sarmiento, K. Fischer, K. G. Lagoudakis, S. Buckley, A. Y. Piggott, and J. Vučković, Nonclassical higher-order photon correlations with a quantum dot strongly coupled to a photonic-crystal nanocavity, Phys. Rev. A **90**, 023846 (2014).

[20] F. Bello and D. M. Whittaker, Photon antibunching and nonlinear effects for a quantum dot coupled to a semiconductor cavity, Phys. Rev. B **82**, 115328 (2010).

[21] Y. X. Liu, A. Miranowicz, Y. B. Gao, J. Bajer, C. P. Sun, and F. Nori, Qubit-induced phonon blockade as a signature of quantum behavior in nanomechanical resonators, Phys. Rev. A **82**, 032101 (2010).

[22] A. Reinhard, T. Volz, M. Winger, A. Badolato, K. J. Hennessy, E. L. Hu, and A. Imamoglu, Strongly correlated photons on a chip, Nat. Photon. **6**, 93 (2011).

[23] A. Majumdar, M. Bajcsy, A. Rundquist, and J. Vučković, Loss-Enabled Sub-Poissonian Light Generation in a Bimodal Nanocavity, Phys. Rev. Lett. **108**, 183601 (2012); A. Majumdar, M. Bajcsy, and J. Vučković, Phys. Rev. A **85**, 041801(R) (2012).

[24] P. Rabl, Photon blockade effect in optomechanical systems, Phys. Rev. Lett. **107**, 063601 (2011); X.-W. Xu and Y.-J. Li, Antibunching photons in a cavity coupled to an optomechanical system, J. Phys. B **46**, 035502 (2013); V. Savona, Unconventional photon blockade in coupled optomechanical systems, arXiv:1302.5937.

[25] J. Q. Liao and F. Nori, Photon blockade in quadratically coupled optomechanical systems, Phys. Rev. A **88**, 023853 (2013).

[26] M. Bradford and J.-T. Shen, Architecture dependence of photon antibunching in cavity quantum electrodynamics, Phys. Rev. A **92**, 023810 (2015).

[27] C. M. Bender and S. Boettcher, Real Spectra in Non-Hermitian Hamiltonians Having $\mathcal{PT}$ Symmetry, Phys. Rev. Lett. **80**, 5243 (1998).

[28] C. M. Bender, Making sense of non-Hermitian Hamiltonians, Rep. Prog. Phys. **70**, 947 (2007).

[29] C. M. Bender, M. Gianfreda, Ş. K. Özdemir, B. Peng, and L. Yang, Twofold transition in $\mathcal{PT}$-symmetric coupled oscillators, Phys. Rev. A **88**, 062111 (2013).

[30] R. El-Ganainy, K. G. Makris, D. N. Christodoulides, and Z. H. Musslimani, Theory of coupled optical $\mathcal{PT}$-symmetric structures, Opt. Lett. **32**, 2632 (2007); K. G. Makris, R. El-Ganainy, D. N. Christodoulides, and Z. H. Musslimani, Beam Dynamics in $\mathcal{PT}$ Symmetric Optical Lattices, Phys. Rev. Lett. **100**, 103904 (2008); Z. H. Musslimani, K. G. Makris, R. El-Ganainy, and D. N. Christodoulides, Optical Solitons in $\mathcal{PT}$ Periodic Potentials, *ibid.* **100**, 030402 (2008); K. G. Makris, R. El-Ganainy, D. N. Christodoulides, and Z. H. Musslimani, $\mathcal{PT}$-Symmetric Optical Lattices, Phys. Rev. A **81**, 063807 (2010).

[31] R. El-Ganainy, M. Khajavikhan, and L. Ge, Exceptional points and lasing self-termination in photonic molecules, Phys. Rev. A **90**, 013802 (2014).

[32] L. Feng, M. Ayache, J. Huang, Y.-L. Xu, M.-H. Lu, Y.-F. Chen, Y. Fainman, and A. Scherer, Nonreciprocal light propagation in a silicon photonic circuit, Science **333**, 729 (2011).

[33] B. Peng, Ş. K. Özdemir, F. Lei, F. Monifi, M. Gianfreda, G. L. Long, S. Fan, F. Nori, C. M. Bender, and L. Yang, Parity-time-symmetric whispering-gallery microcavities, Nat. Phys. **10**, 394 (2014).

[34] L. Chang, X. Jiang, S. Hua, C. Yang, J. Wen, L. Jiang, G. Li, G. Wang, and M. Xiao, Parity-time symmetry and variable optical isolation in active-passive-coupled microresonators, Nat. Photon. **8**, 524 (2014).

[35] X. Liu, S. D. Gupta, and G. S. Agarwal, Regularization of the spectral singularity in $\mathcal{PT}$-symmetric systems by all-order nonlinearities: Nonreciprocity and optical isolation, Phys. Rev. A **89**, 013824 (2014).

[36] B. Peng, Ş. K. Özdemir, S. Rotter, H. Yilmaz, M. Liertzer, F. Monifi, C. M. Bender, F. Nori, and L. Yang, Loss-induced suppression and revival of lasing, Science **346**, 328 (2014).

[37] L. Feng, Z. J. Wong, R.-M. Ma, Y. Wang, and X. Zhang, Single-mode laser by parity-time symmetry breaking, Science **346**, 972 (2014).

[38] H. Hodaei, M.-A. Miri, M. Heinrich, D. N. Christodoulides, and M. Khajavikhan, Parity-time-symmetric microring lasers, Science **346**, 975 (2014).

[39] A. Guo, G. J. Salamo, D. Duchesne, R. Morandotti, M. Volatier-Ravat, V. Aimez, G. A. Siviloglou, and D. N. Christodoulides, Observation of $\mathcal{PT}$-Symmetry Breaking in Complex Optical Potentials, Phys. Rev. Lett. **103**, 093902 (2009).

[40] H. Jing, Ş. K. Ödemir, Z. Geng, J. Zhang, X.-Y. Lü, B. Peng, L. Yang, and F. Nori, Optomechanically-induced transparency in parity-time-symmetric microresonators, Sci. Rep. **5**, 9663 (2015).

[41] C. E. Rüter, K. G. Makris, R. El-Ganainy, D. N. Christodoulides, M. Segev, and D. Kip, Observation of parity-time symmetry in optics, Nat. Phys. **6**, 192 (2010).

[42] A. Regensburger, C. Bersch, M.-A. Miri, G. Onishchukov, D. N. Christodoulides, and U. Peschel, Parity-time synthetic photonic lattices, Nature (London) **488**, 167 (2012).

[43] Z. Lin, H. Ramezani, T. Eichelkraut, T. Kottos, H. Cao, and D. N. Christodoulides, Unidirectional Invisibility Induced by $\mathcal{PT}$-Symmetric Periodic Structures, Phys. Rev. Lett. **106**, 213901 (2011).

[44] H. Ramezani, T. Kottos, R. El-Ganainy, and D. N. Christodoulides, Unidirectional nonlinear $\mathcal{PT}$-symmetric optical structures, Phys. Rev. A **82**, 043803 (2010).

[45] H. Jing, Ş. K. Özdemir, X.-Y. Lü, J. Zhang, L. Yang, and F. Nori, $\mathcal{PT}$-Symmetric Phonon Laser, Phys. Rev. Lett. **113**, 053604 (2014).

[46] J. Zhang, B. Peng, Ş K. Özdemir, Y.-X. Liu, H. Jing, X.-Y. Lü, Y.-L. Liu, L. Yang, and F. Nori, Giant nonlinearity via breaking parity-time symmetry: A route to low-threshold phonon diodes, Phys. Rev. B **92**, 115407 (2015).

[47] X.-Y. Lü, H. Jing, J.-Y. Ma, and Y. Wu, $\mathcal{PT}$-Symmetry-Breaking Chaos in Optomechanics, Phys. Rev. Lett. **114**, 253601 (2015).

[48] Z.-P. Liu, J. Zhang, Ş K. Özdemir, B. Peng, H. Jing, X.-Y. Lü, C.-W. Li, L. Yang, F. Nori, and Y.-X. Liu, Metrology with $\mathcal{PT}$-symmetric cavities: Enhanced sensitivity near the $\mathcal{PT}$ phase transition, arXiv:1510.05249.

[49] J. Vučković, Quantum optics and cavity QED with quantum dots in photonic crystals, arXiv:1402.2541.

[50] In fact, several specific systems have shown nonlinear optical properties that can be mapped under appropriate conditions. (i) It is well known that the Hamiltonian of a two-level quantum emitter interacting with the cavity mode in the limit of large detuning between the cavity mode and the two-level transition can exhibit this effective Kerr nonlinearity when the two-level system remains in its ground state [21]. (ii) Such Kerr nonlinearity can be generated via an optomechanical system in which the optical density inside the cavity is coupled to the displacement of a mechanical oscillator. See, e.g., S. Aldana, C. Bruder, and A. Nunnenkamp, Equivalence between an optomechanical system and a Kerr medium, Phys. Rev. A **88**, 043826 (2013). (iii) Also, strong $\chi^{(3)}$ Kerr nonlinearity can be achieved with an intracavity four-level atomic ensemble driven by a strong laser in dark-sate resonance, as suggested in Ref. [1].

[51] A. Majumdar, M. Bajcsy, D. Englund, and J. Vučković, All optical switching with a single quantum dot strongly coupled to a photonic crystal cavity, IEEE J. Sel. Top. Quantum Electron. **18**, 1812 (2012).

[52] A. Laucht, J. M. Villas-Bôs, S. Stobbe, N. Hauke, F. Hofbauer, G. Böm, P. Lodahl, M.-C. Amann, M. Kaniber, and J. J. Finley, Mutual coupling of two semiconductor quantum dots via an optical nanocavity, Phys. Rev. B **82**, 075305 (2010).

[53] A. Auffèves, D. Gerace, J.-M. Gérard, M. França Santos, L. C. Andreani, and J.-P. Poizat, Controlling the dynamics of a coupled atom-cavity system by pure dephasing, Phys. Rev. B **81**, 245419 (2010).

[54] A. Majumdar, N. Manquest, A. Faraon, and J. Vučković, Theory of electro-optic modulation via a quantum dot coupled to a nano-resonator, Opt. Express **18**, 3974 (2010).

[55] T. K. Fryett, C. M. Dodson, and A. Majumdar, Cavity enhanced nonlinear optics for few photon optical bistability, Opt. Express **23**, 16246 (2015).

[56] M. O. Scully and M. S. Zubairy, *Quantum Optics* (Cambridge University Press, Cambridge, 1997).

[57] K. J. Vahala, Optical microcavities, Nature (London) **424**, 839 (2003).

[58] K. J. Vahala, *Optical Microcavities* (World Scientific, Singapore, 2004), Vol. 5.